The Effect of Chemical States of Dopants on the Microstructures and Band Gaps of Metal-Doped ZrO_2 Thin Films at Different Temperatures

Sue-min Chang and Ruey-an Doong*

Department of Atomic Science, National Tsing Hua University, 101, Sec. 2, Kuang Fu Road, Hsinchu, 30013, Taiwan

Received: June 14, 2004; In Final Form: September 2, 2004

The microstructures and band gaps of sol−gel-derived ZrO_2 thin films incorporating seven-transition-metal ions (Cr^{3+}, Mn^{2+}, Fe^{3+}, Co^{2+}, Ni^{2+}, Cu^{2+}, and Zn^{2+}) were investigated at 550 and 950 °C. Results obtained in this study indicate that the chemical states of the dopants play pivotal roles in controlling the physicochemical properties of the metal-doped ZrO_2 thin films at different temperatures. The reduction of Cr^{3+} and Co^{2+} to zerovalent metals expanded the *d* spacings and enlarged the crystallite sizes in the doped ZrO_2 thin films at 550 °C, while the incorporation of Mn^{2+}, Fe^{3+}, Ni^{2+}, Cu^{2+}, and Zn^{2+} contracted the *d* spacings of the ZrO_2 lattices in the solid solutions. The solubility of the dopants in the ZrO_2 lattices decreased at 950 °C, and this phenomenon induced an m-tetragonal-to-monoclinic phase transformation in the doped ZrO_2. The phase transformation was suppressed in the Cr-, Fe-, and Cu-doped ZrO_2 thin films as a result of the reduction of Cr^{3+} and Fe^{3+} to species having larger sizes than Zr^{4+}. Band gaps of ZrO_2 were reduced in the doped ZrO_2 thin films. The newly generated band gaps of these solid solutions at 550 °C were highly dependent on the d-electronic configurations of the dopants. On the other hand, the segregated metal oxides or zerovalent metals from the ZrO_2 lattice at 950 °C dominated the band gaps of the doped ZrO_2 thin films. Dehydroxylation and deoxygenation processes drove the reduction of metal ions during the thermal treatment. The metal ions having d^5 and d^{10} configurations in the ZrO_2 lattice possessed high stability against thermally induced reductions, while the other ions tended to be reduced in the sol−gel-derived ZrO_2 matrix.

Introduction

Zirconium dioxide (ZrO_2) is one of the most promising catalysts widely used in the petroleum industry for the deformation, dehydrogenation, and isomerization of organic compounds.[1,2] The wide band gap and suitable redox potentials in bands also make ZrO_2 an attractive photocatalyst for the decomposition and mineralization of a wide variety of pollutants.[3,4] Several studies have reported that incorporation of transition-metal ions in the first series (including Fe, V, and Ni) can effectively enhance the efficiency of ZrO_2-based catalytic systems.[5−7] The effects that dopants have on the performance of ZrO_2 are mainly associated with modifying the microstructures including phases and crystallite sizes as well as the reducing band gaps.[5−8]

ZrO_2 exists in three polymorphs: monoclinic, tetragonal, and cubic.[9] Incorporation of metal ions into the ZrO_2 lattice can stabilize the tetragonal phase, which is only stable above 1200 °C, at room temperature because of introduced lattice defects.[10,11] The types of dopants determine the stability of m-tetragonal phase in the metal-doped ZrO_2 at elevated temperatures. Previous studies have demonstrated that m-tetragonal ZrO_2 is maintained at up to 950 °C in Sc-doped ZrO_2 film,[12] while the high stability of m-tetragonal ZrO_2 is observed at 1050 °C in lanthanide-doped ZrO_2 thin films.[13] Such effects may be related to different distortion in the metal-doped ZrO_2 microstructures when the ionic sizes of the dopants are different from Zr^{4+}. The unit cell undergoes a contraction when Zr^{4+} is replaced by metal ions that have smaller ionic radii, and vice versa.[14] Ionic sizes of dopants also influence crystallite sizes in doped ZrO_2 samples. Small crystallite sizes of ZrO_2 are usually obtained when the ionic sizes of dopants are largely different from Zr^{4+}.[13] In addition to the influence on the microstructures, the electronic structures of ZrO_2 are also altered by dopants because of introduced energy levels.[15] The energy levels between the intrinsic bands of ZrO_2 can significantly reduce the band gap.[6,16] ZrO_2 is a direct-transition material having the band gap of about 5.0 eV.[17] The wide band gap has been reduced to 2.3 and 2.8 eV, respectively, when 5 wt % of Fe^{3+} or V^{5+} is doped.[6,18] Depending on the types and chemical states of metal ions, the band gaps of metal-doped ZrO_2 thin films varied. The differences in the band gaps are mainly associated with the electronic configurations of the ions, which control the energy levels in the ZrO_2.

To facilitate catalytic systems in various systems, metal-doped ZrO_2 is usually fabricated in thin films. A sol−gel process is one of the methods most frequently used for the fabrication of metal-doped ZrO_2 films because it is simple and available for various dopants in different amounts. Thermal treatment is a necessary step to stabilize and crystallize sol−gel-derived ZrO_2 films. Calcination temperatures have great influence on the microstructures and band gaps of metal-doped ZrO_2 films.[19,20] Such effects include inducing m-tetragonal-to-monoclinic phase transformation and increasing crystallite sizes. A red-shift of 0.25 eV in the band gap of a Y-doped ZrO_2 film has been reported when the calcination temperature increases from 400 to 1200 °C.[21] In addition, studies have reported that the chemical states of metal ions in the ZrO_2 lattice are converted during thermal treatment. The reduction of Zr^{4+} to Zr^{3+} or Zr^{2+} has

* Corresponding author. E-mail: radoong@mx.nthu.edu.tw; tel: +886-3-5726785; fax: +886-3-5718649.

10.1021/jp047440n CCC: $27.50 © 2004 American Chemical Society
Published on Web 10/16/2004

been found to occur after calcination.[22,23] The changes in the chemical states of dopants such as V^{5+}, Cu^{2+}, and Ru^{3+} in the ZrO_2 lattice have been also identified after thermal treatment.[18,24,25] The final chemical states of dopants are temperature-dependent. Indovina et al.[24] reported that Cu^{2+} in the ZrO_2 lattice was reduced to Cu^+ at 473 K and then to Cu^0 at a high temperature. The mechanism of the change in the chemical states of the dopants is related to the reagents used and to the atmosphere during thermal treatment. The redox properties of the metal ions in the metal oxide lattice are governed by their types and chemical states.[26] The thermally induced conversions of chemical states can result in different ionic sizes and electronic configurations of dopants. However, such effects on the microstructures and band gaps of metal-doped ZrO_2 films receive less concern so far.

In this study, the microstructures and band gaps of the sol−gel-derived ZrO_2 thin films doped with seven-transition-metal ions (Cr^{3+}, Mn^{2+}, Fe^{3+}, Co^{2+}, Ni^{2+}, Cu^{2+}, and Zn^{2+}) are systematically investigated at different temperatures. We emphasize mainly the effect of the chemical states of the dopants on these physicochemical properties of doped ZrO_2 thin films. In addition, the mechanism of the conversions of the chemical states and the redox properties of the seven transition metals in the ZrO_2 lattice are discussed.

Experimental Section

The Preparation of Metal-Doped ZrO_2 Thin Films. Pure and metal-doped zirconium dioxide (ZrO_2) thin films were prepared by a sol−gel method. The sol solution was first obtained by dissolving $ZrCl_4$ (4 g; Fluka) by stirring it vigorously in 2-propanol (IPA; 10 mL; Riedel-de Haën, 99.8%, water content < 0.1%) in an ice−water bath, and then diluting the solution with IPA to get a molar ratio of IPA/Zr of 90. The solution was then hydrolyzed fully using a stoichiometric amount of water. Six metallic salts—$Cr(NO_3)_3 \cdot 9H_2O$ (Riedel-de Haën), $Mn(NO_3)_2 \cdot 4H_2O$ (Merck), $FeCl_3 \cdot 6H_2O$ (Ishizu), $CoCl_2 \cdot 6H_2O$ (Merck), $CuCl_2 \cdot 2H_2O$ (Merck), and $Zn(NO_3)_2 \cdot 4H_2O$ (Acrös)—with appropriate amounts were dissolved in the sol solution to obtain doping levels from 2 to 20 atomic percentage (at. %) relative to zirconium. Because Ni is readily precipitated in IPA solution, $NiCl_2$ was first dissolved in a small amount of ethanol (Fluka, 99.8%, water content < 0.05%) and then mixed with the sol solution. All the metal-doped ZrO_2 sol solutions were aged for 24 h at room temperature in sealed centrifuge tubes. Thin ZrO_2 films were obtained by spin-coating a portion of the sol solution (20 μL) onto a 1.4-cm^2 quartz slide at 3000 rpm for 30 s. Prior to the addition of the sol solution, the quartz slides were cleaned using $K_2C_2O_7/H_2SO_4$ solution to remove traces of organic contaminants on the surface. After coating, the thin films were heated at 80 °C for 5 min to evaporate the solvent, and then they were calcined at 550 or 950 °C in air for 12 h.

SEM Characterization. Scanning electron microscopy (SEM; Hitachi S-4700 Type II) was used to determine the morphology and thickness of each thin film. The microscope was operated at an accelerating voltage of 25 kV and the images were collected under a vacuum of 10^{-8} Torr. All samples for SEM analysis were coated with platinum. The ZrO_2 thin films obtained in this study were smooth and had thicknesses of ca. 20 nm (see Supporting Information, Figure S1). The metal-doped ZrO_2 thin films had similar characteristics.

XRD Identification. The crystalline properties of the thin films were identified by X-ray diffraction (XRD; MAC Science, MXP18) using Cu Kα radiation (λ = 1.5405 Å) and operating at an accelerating voltage of 40.0 kV and an emission current of 150.0 mA. XRD patterns were obtained using an X-ray incident angle of 1.0° and the diffraction signal at 2θ was detected from 25 to 70° using a sampling width of 0.020° and a scanning speed of 4.0°/min.

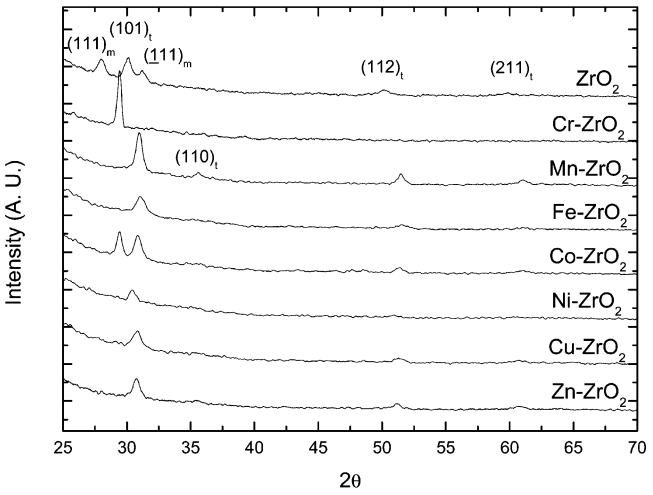

Figure 1. XRD patterns of pure and doped ZrO_2 thin films that had been calcined at 550 °C in air for 12 h.

UV−Visible Spectroscopy. The absorption measurements were performed using a UV−vis spectrometer (Shimadzu, S 1600). Thin film samples were fixed on the light source path. The absorption spectra were recorded in the range from 800 to 200 nm using quartz as the reference. The scanning wavelengths (λ) were then converted into photon energies (E, eV) using the relationship of $E = 1240/\lambda$. The differences in absorbance (ΔA) between the doped and pure ZrO_2 films were calculated ($\Delta A = A_{doped} - A_{pure}$) to characterize the influence that the dopants had on the optical properties of the ZrO_2 film.

XPS Measurements. The X-ray photoelectron spectroscopy (XPS) measurements were performed using a Physical Electronics ESCA PHI 1600 instrument equipped with an Al Kα X-ray source (1486.6 eV). The spherical capacitor analyzer equipped with a multichannel detector had a takeoff angle of 70° relative to the horizon of the sample plane. The photoelectrons were collected into the analyzer at a passing energy of 23.5 eV and the collection step was 0.1 eV. All of the analytical processes were performed under ultrahigh vacuum conditions (maintained $< 1.4 \times 10^{-8}$ Torr). The XPS spectra were acquired after using soft argon etching to remove a 2-nm thickness from the top of the thin films. The binding energy was referenced to the Zr($3d_{5/2}$) at 182.5 eV. The oxidation states were identified according to the binding energy, the doublet separation energy ($\Delta E = BE_p\ 2p_{3/2} - BE_p\ 2p_{1/2}$), and the auger parameter ($\alpha = BE_p - BE_a$).

Results

Crystalline Properties of Metal-Doped ZrO_2 Films at Different Temperatures. Figure 1 presents the XRD patterns of the pure and 20 at. % metal-doped ZrO_2 thin films calcined at 550 °C. The peaks of the $(101)_t$, $(111)_m$, and $(\bar{1}11)_m$ profiles centered at 30.2°, 28.2°, and 31.4° 2θ positions clearly indicate the coexistence of metastable tetragonal and monoclinic phases in the pure ZrO_2 film. Only the metastable tetragonal phase was identified, however, in the metal-doped ZrO_2 samples. No diffraction peaks corresponding to the metal oxides of the dopants were observed in the XRD spectra, suggesting that the dopants were dispersed well in the ZrO_2 matrix. To further identify whether a solid solution was formed, the changes in the d spacing of the $(101)_t$ profile in the ZrO_2 thin film doped with various amounts of Fe and Mn were examined (see

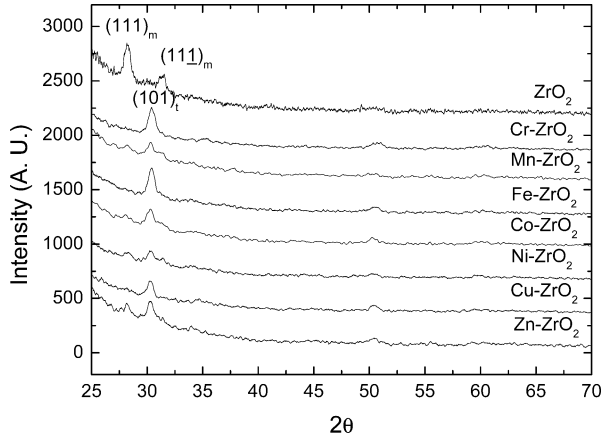

Figure 2. XRD patterns of pure and doped ZrO_2 thin films that had been calcined at 950 °C in air for 12 h.

TABLE 1: The *d* spacings of the $(101)_t$ Profile and the Crystallite Sizes of the Pure and Doped ZrO_2 Thin Films

sample	*d*-spacing (pm)	crystallite size (nm)
ZrO_2	295	15.6
Cr−ZrO_2	304	27.1
Mn−ZrO_2	289	14.2
Fe−ZrO_2	288	10.5
Co−ZrO_2	290, 303	12.5, 17.5
Ni−ZrO_2	293	14.0
Cu−ZrO_2	290	10.4
Zn−ZrO_2	290	13.4

Supporting Information, Figure S2). Linear relationships existed between the *d* spacings and the concentrations of the dopants, which follow Vegard's law,[14] in the Mn- and Fe-doped ZrO_2 films, indicating that the substitutional solid solutions were formed at 550 °C.

Table 1 lists the *d* spacings of the $(101)_t$ profile and the crystallite sizes in the pure and doped ZrO_2 films at 550 °C. The *d* spacing of the pure ZrO_2 was 295 pm and it varied when doped with different metal ions. The *d* spacings of the Mn-, Fe-, Ni-, Cu-, and Zn-doped ZrO_2 thin films were in the range of 288−291 pm, which indicate that shrinkage occurs after doping. In contrast, an expansion of *d* spacing to 304 pm occurred when Cr was doped. Two $(101)_t$ peaks with the *d* spacings of 303 and 290 pm, respectively, appeared in the Co-doped ZrO_2 thin film, depicting that both shrinkage and expansion in the *d* spacing concurrently occurred. The different changes in the microstructure infer that two kinds of Co species might exist in the doped ZrO_2. Similar to the changes in the *d* spacings, the crystallite sizes in the ZrO_2 thin films also increased or decreased depending on the nature of the dopants. The crystallite sizes in the pure and metal-doped ZrO_2 thin films were estimated from the full width at half-maximum (fwhm) of the $(101)_t$ peak using Scherrer's formula.[27] The crystallite size of the $(101)_t$ profile in pure ZrO_2 thin film was calculated to be 15.6 nm. Incorporation of Mn^{2+}, Fe^{3+}, Ni^{2+}, Cu^{2+}, and Zn^{2+} reduced the crystalline sizes to 10.4−14.2 nm, whereas larger crystallite sizes, ranging between 27.1 and 17.5 nm, were obtained in the Cr- and Co-doped ZrO_2 thin films. In addition, preferred orientations of the $(101)_t$ profiles with *d* spacings of 304 and 303 pm, respectively, were also observed in the Cr- and Co-doped ZrO_2 films. Such preferred orientation did not appear, however, in the other metal-doped ZrO_2 thin films.

Figure 2 presents the XRD patterns of the pure and doped ZrO_2 films calcined at 950 °C. The pure monoclinic phase, which was transformed from the m-tetragonal phase, was observed in the pure ZrO_2 thin film at 950 °C, but this phase

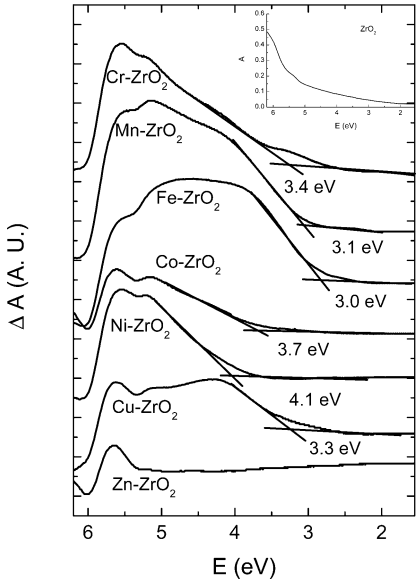

Figure 3. UV−vis absorption spectra of the ZrO_2 thin film and the difference absorption spectrum between the pure and metal-doped ZrO_2 thin films calcined at 550 °C.

transformation was suppressed in the presence of dopants. The XRD patterns indicate that m-tetragonal phases remained in the doped ZrO_2 thin films after calcination at 950 °C and only a small fraction of crystals existed as the monoclinic phase in the Mn-, Co-, Ni-, and Zn-doped ZrO_2 thin films. The *d* spacings of the $(111)_m$ profiles in the doped ZrO_2 calcined at 950 °C ranged between 315 and 317 pm; these values are close to that of pure ZrO_2 (316 pm). Similarly, the *d* spacings of the $(101)_t$ profiles in the doped ZrO_2 thin films (294−295 pm) were also close to that of the pure ZrO_2 film (295 pm). These results reveal that the dopants segregate from the ZrO_2 lattices at the elevated temperature.

Spectroscopic Properties of Metal-Doped ZrO_2 Films at Different Temperatures. The band gaps (E_g) of the pure and doped ZrO_2 thin films were determined from their UV−vis absorption spectra. Figure 3 displays the absorption curves of the pure ZrO_2 film and the difference in absorbance ($\Delta A = A_{doped} - A_{undoped}$) between the pure and 20 at. % doped ZrO_2 films calcined at 550 °C. The pure ZrO_2 thin film showed a steep increase in the absorption at the energy region >5.5 eV. The direct band gap of 5.7 eV for the ZrO_2 film was determined from the onset of the absorption (see Supporting Information, Figure S3). With the exception of the Zn-doped ZrO_2 thin film, the increase in ΔA at the energy region <5.7 eV was observed in all of the doped ZrO_2 thin films, indicating that red-shifts exist in the doped ZrO_2 thin films. On the basis of these absorption edges of the red-shifts, the reduced band gaps in the doped ZrO_2 thin films were determined. The absorption edges of the Cr-, Mn-, Fe-, Co-, Ni-, and Cu-doped ZrO_2 samples calcined at 550 °C were located at the excitation energies of 3.4, 3.1, 3.0, 3.7, 4.1, and 3.3 eV, respectively. No obvious difference in absorbance between the Zn-doped and pure ZrO_2 films was observed, depicting that the impurity level of Zn^{2+} is close to the conduction or valence band of ZrO_2.

Figure 4 presents the absorption curve of the pure ZrO_2 film and the difference in absorbance ($\Delta A = A_{doped} - A_{undoped}$) between the pure and metal-doped ZrO_2 films calcined at 950 °C. The ZrO_2 film calcined at 950 °C showed two direct band-to-band transitions with the band gaps of 5.1 and 5.9 eV (see Supporting Information, Figure S3). The Cr-, Mn-, Fe-, and Ni-doped ZrO_2 films showed red-shifts in the absorption spectra;

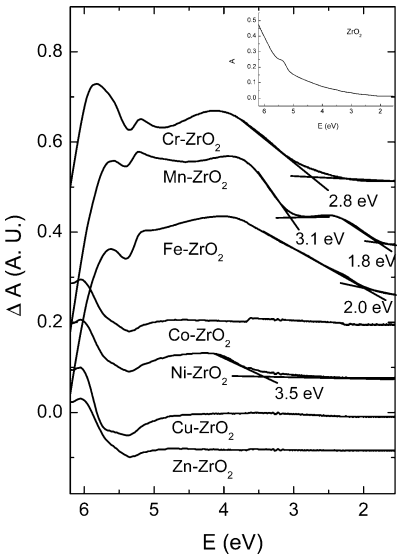

Figure 4. UV−vis absorption spectra of the ZrO_2 thin film and the difference absorption spectrum between the pure and metal-doped ZrO_2 thin films calcined at 950 °C.

however, no obvious shifts in photon energies were observed in the Co-, Cu-, and Zn-doped ZrO_2 thin films. The red-shifts in the Cr-, Fe-, and Ni-doped ZrO_2 thin films began at 2.8, 2.0, and 3.5 eV, respectively, and two absorption bands having the onsets at 3.1 and 1.8 eV were observed in the spectra of the Mn-doped ZrO_2 sample. The metal-doped ZrO_2 thin films calcined at 950 °C display smaller band gaps than those calcined at 550 °C. This discrepancy may be attributed to conversions in the chemical states of the dopants upon thermal treatment. In addition, two absorptions in the Mn-doped ZrO_2 film also infer that possibly two kinds of Mn species are formed at 950 °C. Therefore, the chemical states of the seven dopants in the ZrO_2 thin films at different temperatures were further examined by using XPS.

Chemical States of the Dopants at Different Temperatures. The chemical states of the dopants in the thin films were identified after removing a 2-nm thickness from the top of each thin film. Table 2 summarizes the chemical states of the dopants in the doped ZrO_2 films at 80−950 °C. The percentages of the species were calculated from the ratios of the peak areas of each peak in the XPS spectra. Results indicate that Fe^{3+}, Co^{2+}, Ni^{2+}, and Cu^{2+} had already reduced to Fe^{2+}, Co^0, Ni^0, and Cu^+, respectively, prior to calcination. These reductions occurred in conjunction with the oxidation of 2-propanol to acetone under the suitable redox conditions (see Supporting Information, Table 1S). After calcination at 550 °C, Cu^+ was still the major oxidation state, while Fe^{2+} was oxidized and reduced to Fe^{3+} and Fe^0, respectively, in an atomic ratio of 75:25. The fraction of Co^0 increased from 36 to 49% after calcination implies that some Co^{2+} was reduced upon thermal treatment. Moreover, the existence of Cr^0 in the Cr-doped ZrO_2 film calcined at 550 °C also suggests that the reduction of Cr^{3+} to Cr^0 resulted during the calcination process. In contrast, the Mn^{2+} and Zn^{2+} ions maintained their original oxidation states after calcination at 550 °C.

To further understand whether the reducing capacity toward the doped metal ions increased at elevated temperatures, the chemical states of the dopants in the doped ZrO_2 films calcined at 950 °C were identified. The results indicate that the Fe^{3+} ions were reduced to Fe^{2+}/Fe^0 in the doped ZrO_2 film at 950 °C. This phenomenon is attributed to the presumed electron transfer that occurs upon the elimination of oxygen in the ZrO_2 lattice.[28] Concurrently, the contents of Cr^0, Co^0, and Ni^0 decreased as the temperature increased from 550 to 950 °C. This situation indicates that oxidation occurred upon calcination at 950 °C. Mn^{2+}, Zn^{2+}, and Cu^+ were not detected in the ZrO_2 thin films after the calcination at 950 °C. However, the atomic ratios of Mn/Zr and Zn/Zr detected in the surface layer were 0.5 and 0.7, respectively, which are higher than their stoichiometric ratio of 0.2 (20 at. %). This observation reveals that the Mn^{2+} and Zn^{2+} ions were segregated from the ZrO_2 lattice and accumulated at the surface of the thin films at 950 °C. The accumulated Zn^{2+} ions retained their original chemical states, whereas some of the Mn^{2+} ions (33%) were oxidized to Mn^{4+} in the surface layer upon exposure to oxygen in air. Such surface accumulation of dopants did not occur in the Cu-doped ZrO_2 thin film because no photoelectrons of Cu were detected at the surface. Presumably, this phenomenon is due to the reduction to Cu^0, which has a strong ability to diffuse into the substrate.[29]

Discussion

In this study, we have found that the conversions in the chemical states of the dopants at different temperatures play important roles in the crystalline properties and band gaps of the metal-doped ZrO_2 thin films. Depending on the ionic sizes of dopants after calcination, the dopants have two effects on the *d* spacings of the ZrO_2 films. The introduction of dopants that have ionic sizes smaller than that of Zr^{4+} (98 pm), which includes Mn^{2+}, Fe^{3+}, Ni^{2+}, Cu^+, and Zn^{2+}, contracted the *d* spacings of the doped ZrO_2 lattices. In contrast, expansion of

TABLE 2: The Binding Energy (BE), Doublet Separation (ΔE), and Chemical States of Dopants in the ZrO_2 Thin Films at Different Temperatures

	as-dried			calcined at 550 °C			calcined at 950 °C		
dopant	BE[a] (eV)	ΔE[b] (eV)	chemical states	BE[a] (eV)	ΔE[b] (eV)	chemical states	BE[a] (eV)	ΔE[b] (eV)	chemical states
Cr	576.6	9.8	Cr^{3+}	574.4	9.2	Cr^0 (75)[c]	574.4	9.2	Cr^0 (54)
				575.8	9.8	Cr^{3+} (25)	576.8	9.8	Cr^{3+} (46)
Mn	641.5	11.4	Mn^{2+}	641.5	11.4	Mn^{2+}	641.3	11.4	Mn^{2+}[d] (67)
							642.5	11.6	Mn^{4+}[d] (33)
Fe	709.5	13.0	Fe^{2+}	707.5	13.0	Fe^0 (25)	707.0	12.6	Fe^0 (35)
				710.9	13.2	Fe^{3+} (75)	709.5	13.0	Fe^{2+} (65)
Co	777.2	15.1	Co^0 (36)	777.1	15.1	Co^0 (49)	777.5	15.0	Co^0 (13)
	780.3	15.4	Co^{2+} (64)	780.4	15.4	Co^{2+} (51)	780.4	15.0	Co^{2+} (87)
Ni	852.0	17.1	Ni^0 (58)	851.7	17.1	Ni^0 (53)	851.8	17.1	Ni^0 (39)
	855.2	17.8	Ni^{2+} (42)	852.8	18.2	Ni^{2+} (47)	854.0	18.2	Ni^{2+} (61)
Cu	932.0	19.7	Cu^+	932.2	19.9	Cu^+			
Zn	1022. 2	23.1	Zn^{2+}	1021. 8	23.3	Zn^{2+}	1021.8	23.0	Zn^{2+}[d]

[a] The binding energy of $2p_{3/2}$ line. [b] ΔE = BE $2p_{3/2}$ − BE $2p_{1/2}$. [c] Values in parentheses are the percentages of the species. [d] The species accumulated in the surface layer.

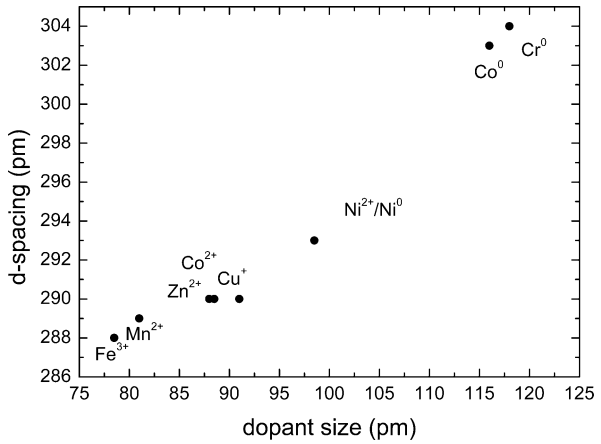

Figure 5. The *d* spacings of the $(101)_t$ profile in the metal-doped ZrO_2 thin films plotted as a function of the radius of the dopants.

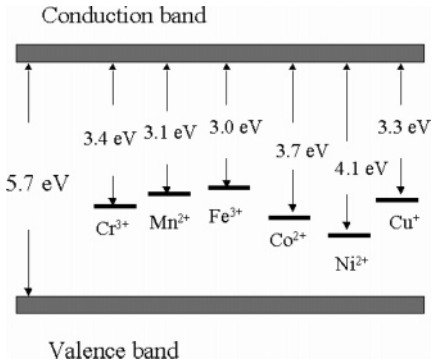

Figure 6. Schematic impurity levels of the transition-metal ions in the ZrO_2 thin films.

the *d* spacings in the Cr- and Co-doped ZrO_2 lattices was due to the reduction of Cr^{3+} and Co^{2+} to the large-sized metallic elements (Cr^0: 118 pm; Co^0: 116 pm). The appearance of both contracted and expanded *d* spacings in the Co-doped ZrO_2 suggests that the Co^{2+} and Co^0 species are included in separated crystal domains. Although about half of the Ni^{2+} ions were reduced to Ni^0 at 550 °C, only one contracted *d* spacing was obtained for the Ni-doped ZrO_2 thin film. This finding indicates that both the Ni^{2+} and Ni^0 species are included in the same crystallite domain and that the averaged dopant size determines the *d* spacing. A positive correlation exists between the dopant sizes and the *d* spacings of ZrO_2 when the solid solutions were formed at 550 °C (Figure 5). In addition, the preferred orientation of the $(101)_t$ profile and the large crystallite sizes in the Cr- and Co-doped ZrO_2 thin films may possibly be due to the expansion of *d* spacings caused by the large metallic sizes.

Unlike the *d* spacings present in the samples calcined at 550 °C, no obvious difference in *d* spacings between the pure and doped ZrO_2 thin films was observed after calcination at 950 °C, which implies that the dopants are segregated from the ZrO_2 lattice. This segregation is attributed to decreases in the solubility of the dopants at elevated temperatures. However, the peaks corresponding to the metal oxides of the dopants were not observed in the XRD patterns, reflecting the fact that the crystallite sizes of the segregated metal oxides in the ZrO_2 matrix was too small to be detected by XRD. Ram[30] investigated the structural properties of Cr-doped ZrO_2 nanoparticles and found that the segregation of dopants could trigger the phase transformation of ZrO_2 from m-tetragonal to monoclinic form. In this study, however, only small fractions of m-tetragonal phase were converted into monoclinic phase in the Mn-, Co-, Ni-, and Zn-doped ZrO_2 films. The fact that the m-tetragonal phases are maintained in the doped ZrO_2 thin films reveals that trace amounts of the dopants are still included in the ZrO_2 lattice even though most of the dopants have segregated. The different stabilities of the m-tetragonal phases in the doped ZrO_2 films are controlled by the conversions of the chemical states of the dopants in the ZrO_2 lattices. When large fractions of dopants are reduced to species that have radii larger than that of Zr^{4+}, such as Cr^0 (118 pm), Fe^0 (117 pm), and Fe^{2+} (106 pm), the stability of the m-tetragonal phase can be maintained. In contrast, the phase is easily transformed to monoclinic form in the metal-doped ZrO_2 thin film when the doped ions have smaller ionic radius, such as those of Mn^{2+}, Co^{2+}, Ni^+, and Zn^{2+}. This phenomenon is attributed to the fact that large-sized dopants can assist the ZrO_2 structure to bear the contraction in lattice volume during the transformation from m-tetragonal phase to monoclinic phase, and thus the stability of the m-tetragonal phase at high temperatures is enhanced. A similar phenomenon has been reported for lanthanide-doped ZrO_2 thin films that stabilize the m-tetragonal phase at temperatures up to 1050 °C.[13]

In addition to the changes in the microstructures, the electronic structures of the metal-doped ZrO_2 thin films also vary at different temperatures. The band gap of the ZrO_2 thin film calcined at 550 °C was 5.7 eV, which is larger than the reported value (5.0 eV).[17] This increase in the band gap is due primarily to a quantum confinement effect when the crystallite size is down to the nanoscale.[21] Incorporation of the metal ions into the ZrO_2 thin films resulted in red-shifts in the absorption spectra. This observation suggests that impurity levels are introduced between the intrinsic bands of the ZrO_2 films, which subsequently generate new band gaps. Photon-induced electron transitions in the doped ZrO_2 can be either transitions between the localized impurity levels and the delocalized conduction band or d−d transitions.[31] In this study, only continuous absorption bands were observed in the difference absorbance (ΔA) spectra, revealing that the transitions between the impurity levels and the conduction band are dominant and the band gaps of the doped ZrO_2 films are dependent on the positions of the impurity levels in the intrinsic band gap. Substantial amounts of metallic Cr, Co, and Ni existed in the ZrO_2 lattices at 550 °C. However, the red-shifts of the Cr-, Co-, and Ni-doped ZrO_2 thin films were inconsistent with the atomic absorption of Cr (357.9 nm), Co (240.7 nm), or Ni (232.0 nm),[32] respectively. This finding suggests that the red-shifts in these thin films are associated mainly with electron transitions from the impurity levels of the remaining Cr^{3+} (25%), Co^{2+} (51%), and Ni^{2+} (47%) to the conduction band. Figure 6 illustrates the energy levels of the impurity ions in the ZrO_2 intrinsic bands at 550 °C. The band gaps of the doped ZrO_2 films are dependent on the d-electronic configurations of the impurity ions. The red-shifts indicate that Mn^{2+} and Fe^{3+}, which have d^5 configurations, have the highest energy levels.

Compared to the situation at 550 °C, the band gaps of the metal-doped ZrO_2 thin films decreased at 950 °C. The changes in the band gaps are related to the segregation and reduction of the dopants. The Fe^{3+} ions, which were stable in the ZrO_2 lattice at 550 °C, were reduced to Fe^{2+} and Fe^0 when the temperature increased to 950 °C. Moreover, the solubility of the dopants decreased and metal oxides or metals segregated from the ZrO_2 lattice at 950 °C. The accumulated Mn at the film surface comprised Mn^{2+} and Mn^{4+} species. The band gaps of 1.8 and 3.1 eV in the Mn-doped ZrO_2 correspond to the band gaps of MnO_2 and MnO, respectively.[33,34] In addition, the Cr- and Fe-doped ZrO_2 thin films had band gaps of 2.8 and 2.0 eV,

respectively; these values are similar to those expected for Cr_2O_3 and FeO.[35,36] On the other hand, the absorption edge at 355 nm for the Ni-doped ZrO_2 is close to the value of the atomic absorption of Ni (352.4 nm). In contrast to the solid solution forms, these results reveal that the band gaps of the dopants in their oxides or metallic forms dominate the new band gaps of the doped ZrO_2 thin films at 950 °C.

When the microstructures and the band gaps of the doped ZrO_2 thin films with respect to the conversions of the chemical states of the dopants have been demonstrated, the mechanisms of the conversions of the chemical states during thermal treatment require further clarification. From the XPS results obtained at different temperatures, the reducing behavior of dopants in the ZrO_2 thin film was observed. The reduction of the doped ions is associated initially with the oxidation of 2-propanol to acetone in the as-dried samples. Afterward, dehydroxylation and deoxygenation processes drive the reduction of the metal ions in the sol−gel-derived ZrO_2 thin films during thermal treatment. The further reduction of Fe^{3+} to Fe^{2+} and Fe^0 from 550 to 950 °C indicates the fact that the reducing capacity to cations was enhanced with increasing temperatures. In contrast to these reductions, oxidations of the dopants also occurred at 950 °C, in which the m-tetragonal phase was converted to the monoclinic phase. This phenomenon is presumably due to this phase transformation being triggered by an intake of oxygen from air.[37] The systematic identification of the chemical states of the dopants depicts that the redox properties of the dopants in the ZrO_2 matrix are highly dependent on their d-electronic configurations. At 550 °C, the dopants that have half-filled (d^5) and closed-shell (d^{10}) d-electron configurations, including Mn^{2+} and Fe^{3+}, Cu^+, and Zn^{2+}, have specially high stability against thermally induced reductions. On the other hand, metal ions that lack these stable electronic structures, such as $Cr^{3+}(d^3)$ and $Co^{2+}(d^7)$, are reduced to metallic elements upon calcination. These results clearly indicate that the conversions of the chemical states change the ionic sizes and electronic configurations of the dopants, which control the microstructures and band gaps of the doped ZrO_2 at different calcination temperatures.

Conclusions

The chemical states, as well as the ionic sizes and d-electronic configurations, of the dopants determine the crystalline properties and band gaps of the metal-doped ZrO_2 thin films. The oxidation of 2-propanol and the dehydroxylation and deoxygenation processes drive the reduction of the metal ions in the sol−gel-derived ZrO_2 thin films at different temperatures. The final oxidation states control the microstructures, including the *d* spacings, the crystallite sizes, the preferred orientation, and the phase transformation, of the metal-doped ZrO_2 thin films. On the other hand, the changes in chemical states lead to different electronic configurations that influence the positions of the impurity levels between the intrinsic bands and the new band gaps of the metal-doped ZrO_2 thin films. The redox properties of the metal ions in the first series are dependent upon the d-electronic configurations and the calcination temperatures. The ions with the d^5 or d^{10} configurations possess high stability in the ZrO_2 lattice while the other ions are readily reduced at elevated temperatures. The results obtained in this study clearly demonstrate that the dopants influence the physicochemical properties of ZrO_2 thin film. This finding should be helpful in facilitating the development of catalytic processes using metal-doped ZrO_2 thin films.

Acknowledgment. We thank the National Science Council, Taiwan, R.O.C. for the financial support under grant No. NSC 92-2113-M007-068.

Supporting Information Available: Descriptions of the morphology and thickness of the sol−gel-derived ZrO_2 thin film, the relationship between *d* spacings and concentrations of the dopants, the direct band gaps of ZrO_2 thin films at different temperatures, and the reducing behavior of the metal ions in the as-dried ZrO_2 thin film. This material is available free of charge via the Internet at http://pubs.acs.org.

References and Notes

(1) Pieck, C. L.; Banares, M. A.; Fierro, J. L. G. *J. Catal.* **2004**, *224*, 1.
(2) Wang, S. B.; Murata, K.; Hayakawa, T.; Hamakawa, S.; Suzuki, K. *Energy Fuels* **2001**, *15*, 384.
(3) Schattka, J. H.; Shchukin, D. G.; Jia, J. G.; Antonietti, M.; Caruso, R. A. *Chem. Mater.* **2002**, *14*, 5103.
(4) Reddy, V. R.; Hwang, D. W.; Lee, J. S. *Korean J. Chem. Eng.* **2003**, *20*, 1026.
(5) Yan, L.; Qing, Y.; Wei, J. M.; Xu, B. Q. *Chinese J. Catal.* **2004**, *25*, 326.
(6) Navio, J. A.; Hidalgo, M. C.; Colon, G.; Botta, S. G.; Litter, M. I. *Langmuir* **2001**, *17*, 202.
(7) Pieck, C. L.; del Val, S.; Granados, M. L.; Banares, M. A.; Fierro, J. L. G. *Langmuir* **2002**, *18*, 2642.
(8) Anpo, M.; Nomura, T.; Kondo, J.; Domen, K.; Maruya, K. I.; Onishi, T. *Res. Chem. Intermed.* **1990**, *13*, 195.
(9) Hannink, R. H. J.; Kelly, P. M.; Muddle, B. C. *J. Am. Ceram. Soc.* **2000**, *83*, 461.
(10) Labaki, M.; Lamonier, J. F.; Siffert, S.; Zhilinskaya, E. A.; Aboukais, A. *Colloids Surf., A* **2003**, *227*, 63.
(11) Rivas, P. C.; Caracoche, M. C.; Pasquevich, A. F.; Martinez, J. A.; Rodriguez, A. M.; Garcia, A. R. L.; Mintzer, S. R. *J. Am. Ceram. Soc.* **1996**, *79*, 831.
(12) Zhang, Y. W.; Jin, S.; Yang, Y.; Liao, C. S.; Yan, C. H. *Solid State Commun.* **2002**, *122*, 439.
(13) Hartridge, A.; Krishna, M. G.; Bhattacharya, A. K. *Thin Solid Films* **2001**, *384*, 254.
(14) West, A. R. *Basic Solid State Chemistry*; John Wiley & Sons: New York, 1998.
(15) Kralik, B.; Chang, E. K.; Louie, S. G. *Phys. Rev. B* **1998**, *57*, 7027.
(16) Navio, J. A.; Colon, G.; Herrmann, J. M. *J. Photochem. Photobiol., A* **1997**, *108*, 179.
(17) Emeline, A.; Kataeva, G. V.; Litke, A. S.; Rudakova, A. V.; Ryabchuk, V. K.; Serpone, N. *Langmuir* **1998**, *14*, 5011.
(18) Adamski, A.; Sojka, Z.; Dyrek, K.; Che, M. *Solid State Ionics* **1999**, *117*, 113.
(19) Ramamoorthy, R.; Ramasamy, S.; Sundararaman, D. *J. Mater. Res.* **1999**, *14*, 90.
(20) Srinivasan, R.; Hubbard, C. R.; Cavin, O. B.; Davis, B. H. *Chem. Mater.* **1993**, *5*, 27.
(21) Kosacki, I.; Petrovsky, V.; Anderson, H. U. *Appl. Phys. Lett.* **1999**, *74*, 341.
(22) Zhao, Q.; Wang, X. P.; Cai, T. X. *Appl. Surf. Sci.* **2004**, *225*, 7.
(23) Nishino, Y.; Krauss, A. R.; Lin, Y. P.; Gruen, D. M. *J. Nucl. Mater.* **1996**, *228*, 346.
(24) Indovina, V.; Occhiuzzi, M.; Pietrogiacomi, D.; Tuti, S. *J. Phys. Chem. B* **1999**, *103*, 9967.
(25) Kristof, J.; Daolio, S.; De Battisti, A.; Piccirillo, C.; Mihaly, J.; Horvath, E. *Langmuir* **1999**, *15*, 1498.
(26) Saadoune, I.; Cora, F.; Alfredsson, M.; Catlow, C. R. A. *J. Phys. Chem. B* **2003**, *107*, 3012.
(27) Stefanic, G.; Stefanic, I. I.; Music, S. *Mater. Chem. Phys.* **2000**, *65*, 197.
(28) Jana, S.; Biswas, P. K. *Mater. Lett.* **1997**, *30*, 53.
(29) Sun, Y. M.; Lee, S. Y.; Lemonds, A.; Lozano, J.; Zhou, J. P.; Ekerdt, J. G.; White, J. M.; Imesh, I. *Surf. Interface Anal.* **2001**, *32*, 79.
(30) Ram, S. *J. Mater. Sci.* **2003**, *38*, 643.
(31) Pankove, J. I. *Optical Processes in Semiconductors*; Dover Publications Inc: New York, 1971.
(32) *Method 7000B: Flame Atomic Absorption Spectrophotometry;* CD-ROM 7000B-1; United States Environmental Protection Agency: Washington, D.C., 1998.
(33) Tian, J. H.; Liang, B. C.; Wang, Y.; Li, S. F. *J. Electroanal. Chem.* **2002**, *526*, 36.
(34) Takahashi, M.; Igarashi, J. *Phys. Rev. B* **1996**, *54*, 13566.
(35) Cheng, R. H.; Xu, B.; Borca, C. N.; Sokolov, A.; Yang, C. S.; Yuan, L.; Liou, S. H.; Doudin, B.; Dowben, P. A. *Appl. Phys. Lett.* **2001**, *79*, 3122.
(36) Zimmermann, R.; Steiner, P.; Claessen, R.; Reinert, F.; Hufner, S.; Blaha, P.; Dufek, P. *J. Phys.: Condens. Matter* **1999**, *11*, 1657.
(37) Collins, D. E.; Bowman, K. J. *J. Mater. Res.* **1998**, *13*, 1230.